Journal of Food Engineering 237 (2018) 183–193

Contents lists available at ScienceDirect

Journal of Food Engineering

journal homepage: www.elsevier.com/locate/jfoodeng

Sensitivity analysis using a model based on computational fluid dynamics, discrete element method and discrete phase model to study a food hydrofluidization system

Jesica D. Orona, Susana E. Zorrilla, Juan Manuel Peralta*

Instituto de Desarrollo Tecnologico para la Industria Quimica (INTEC), Universidad Nacional del Litoral – CONICET, Guemes 3450, S3000GLN, Santa Fe, Argentina

ARTICLE INFO

Keywords:
Hydrofluidization
DEM
DPM
CFD
Food
Sensitivity analysis

ABSTRACT

A sensitivity analysis was performed to study a hydrofluidization system, using a previous partially validated model that considers multiple fluid immersed jets and moving food spheres. The inputs were the average velocity of jets at the orifices (*V*), the refrigerating medium temperature (*T*), the distance between orifices (*S*), and the number of spheres (*E*). The outputs were the fluid and spheres velocities, the turbulence level, the dispersion level of the spheres, and the mass and heat transfer in the food. In general, the transfer phenomena in the fluid were mainly affected by *E*, *S* and *V*. In the food, the energy transfer was influenced by all variables, while its mass counterpart mainly depended on *T*. This study showed that a combination of computational fluid dynamics, a discrete element method and a discrete phase model is a simple but powerful tool to simulate food processing systems with relatively low computational requirements.

1. Introduction

As mentioned in a recent review by James et al. (2015), hydrofluidization (HF) is one of the novel freezing technologies designed to improve the economics and production quality of frozen foods, originally developed by Fikiin (1992) and Fikiin and Fikiin (1998). This technology uses an unfreezable liquid which is pumped through orifices or nozzles in a vessel to create agitating immersed liquid jets (Fikiin and Fikiin, 1998). The highly turbulent liquid and moving products ensure therefore extremely high surface heat transfer coefficients and high freezing rates (Fikiin, 2003, 2008; Fikiin and Fikiin, 1998).

The modeling approach of HF has evolved through different configurations (Belis et al., 2015; Peralta et al., 2007, 2009, 2010, 2012; Verboven et al., 2003). Although, the main heat and mass transfer parameters were thoroughly studied and related to the operative variables, the movement of the particles and its effect on the transport phenomena needed to be modeled. On one hand, computational fluid dynamics (CFD) represents a powerful tool that helps to describe fluid systems and their main heat and mass transfer variables. Its versatility allows researchers to use it to design, operate and optimize fluid systems (Norton and Sun, 2010; Thévenin and Janiga, 2008). On the other hand, the discrete phase model (DPM) and the discrete element method (DEM) are novel techniques used to estimate the particle movement in fluid systems (Fryer et al., 2011; Norton and Sun, 2007; Tsotsas and Mujumdar, 2014).

Recently, Orona et al. (2017) developed a model that additionally takes into account mobile foods. The strategy consists in combining CFD with DPM and DEM. DPM allows tracking the food spheres through the flow field calculated by CFD while DEM allows obtaining information related to sphere-sphere and sphere-wall interactions. The model was completed with the necessary parameters, the restitution coefficients being experimentally obtained. The combination of CFD-DPM-DEM applied to a study case of 13 potato spheres in a domain with 69 immersed jets within a representative operative scenario allowed studying the main features of the system.

Although, the proof of concept presented by Orona et al. (2017) laid the groundwork for the use of DEM as a tool to study HF systems, a detailed investigation of the individual and combined effect of the main operative variables on the heat and mass transfer (i.e. sensitivity analysis) is needed. The objective of this work was to study a HF system through a sensitivity analysis of the main variables involved using the model described by Orona et al. (2017). This methodology will improve the understanding of HF systems by analyzing the effect of the main operative variables ranged within the values commonly found in the literature on the main phenomena involved.

* Corresponding author.
E-mail address: jmperalta@intec.unl.edu.ar (J.M. Peralta).

https://doi.org/10.1016/j.jfoodeng.2018.05.019
Received 2 November 2017; Received in revised form 11 May 2018; Accepted 22 May 2018
Available online 23 May 2018

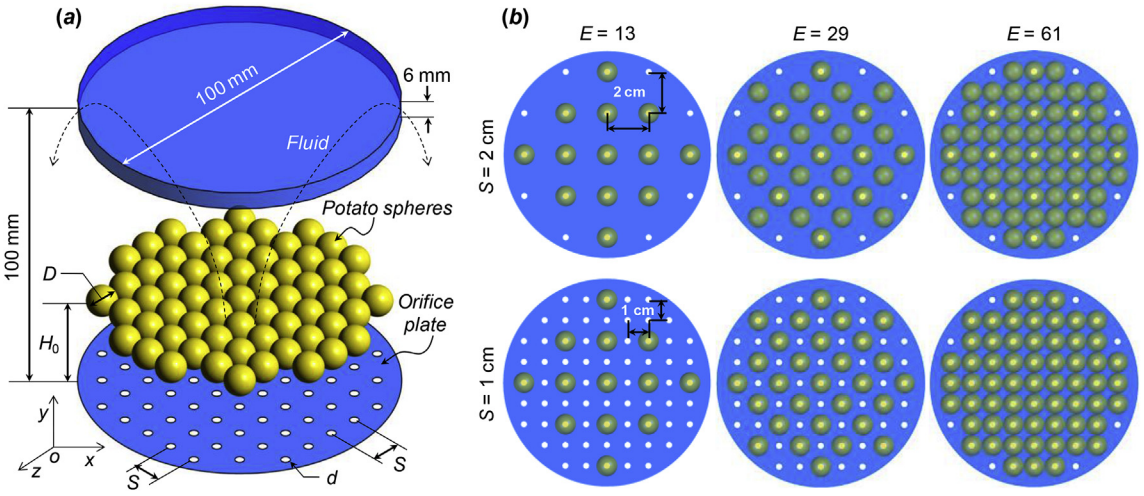

Fig. 1. (*a*) Schematic diagram of the hydrofluidization system studied and (*b*) geometric arrays of orifices and spheres used in this study.

2. Materials and methods

2.1. System studied

The studied hydrofluidization system was described by Orona et al. (2017). Briefly, it consisted of a cylindrical vessel of 100-mm diameter and 100-mm in height and a plate with 3-mm diameter (d) round orifices to produce jets at its base (Fig. 1*a*). A regularly spaced squared array of 10-mm diameter (D) spheres initially placed at a distance H_0 of 50 mm from the orifice plate was used. The liquid-air interface was considered as an adiabatic wall to simplify computations (Orona et al., 2017). As food samples, spheres were considered made by potato (*Solanum tuberosum* L.). As refrigerating medium, an aqueous solution of NaCl 0.231 kg kg^{-1} (w/w) was considered.

2.2. Geometric arrays and operative conditions studied (inputs)

The orifices to produce jets were squared arrays of 21 orifices (minimum distance among the geometric orifice centers, $S = 2$ cm) and 69 orifices ($S = 1$ cm), while the spheres were regularly spaced in squared arrays of 13, 29, and 61 spheres ($E = 13$, $E = 29$, $E = 61$, respectively) (Fig. 1*b*).

The operative conditions studied were the refrigerating medium temperature ($T = -5$ °C, $T = -10$ °C) and average velocity of the refrigerating medium at the orifices ($V = 0.30$ m s^{-1}, $V = 0.59$ m s^{-1}, $V = 1.18$ m s^{-1}). The conditions studied are codified as T*xx*V*xxx*S*x*E*xx*, where the *x*'s are replaced by the absolute values of the operative conditions used. For example T5V030S1E13 refers to the condition where $T = -5$ °C, $V = 0.30$ m s^{-1}, $S = 1$ cm and $E = 13$.

2.3. Mathematical modeling of the transport phenomena

The mathematical modeling of the transport phenomena of the system studied was thoroughly described by Orona et al. (2017). Briefly, each simulation consisted in first solving the fluid phase using the Continuity and Navier-Stokes equations through CFD until steady state conditions were obtained (3 s of simulated time). Turbulence was modeled using the $\kappa - \omega$ SST model. Then, spheres were injected at positions described in Fig. 1 and particle interactions (particle-fluid, particle-particle and particle-wall) were solved using a combination of CFD, DPM and DEM (additional 5 s of simulated time). When spheres appear in the domain, heat and mass transfer in the solid and fluid domain were solved. Each time step consisted in: (*a*) the heat, mass and momentum transfer in the liquid refrigerating medium by combining CFD with DPM and DEM, and then, (*b*) the heat and mass transfer inside the food sample. In the first step, the velocity and position of the particles are estimated through DPM and DEM. An average surface heat transfer coefficient for each sphere is obtained and used to transfer information from the liquid to the solid phase. In the second step, a heat and mass transfer model proposed in previous studies (Peralta et al., 2010, 2012; Zorrilla and Rubiolo, 2005a, 2005b) is used.

It is worth recalling that DPM allows estimating the velocity vector of each sphere accounting different forces: the drag force per unit sphere mass F_D (Gidaspow, 1994) and the force per unit sphere mass due to interactions between spheres or between spheres and the domain wall $\underline{F}_{DEM}$, composed by the normal component $\underline{F}_N$ and the tangential component $\underline{F}_T$. Particularly, DEM accounts for forces $\underline{F}_{DEM}$ (Crowe et al., 2012). In Table 1, the main data used for simulation in DEM are shown. Additional details related to the computational domain, the partial validation process and conditions of the simulations are thoroughly discussed by Orona et al. (2017).

2.4. Variables analyzed (outputs)

In Table 2, a summary of the variables analyzed is shown. The main features related to those expressions can be found in Orona et al. (2017).

3. Results and discussion

3.1. Mesh independence test

The mesh independence was checked by Orona et al. (2017) using the local values of $\langle v_p \rangle$, $\langle v_f \rangle$ at 3 s, $\langle Tu \rangle$ at 3 s, and $\langle h_c \rangle$ at 3 s, as reference variables. A mesh composed of 170770 elements was considered appropriate for simulations.

Table 1
Data used for simulations in DEM.

Force	Data	Source
$\underline{F}_N$	$K = 10{,}000$ s^{-2}	(a)
	$\eta_w = 0.52$	(b)
	$\eta_p = 0.77$	(b)
$\underline{F}_T$	$\mu_{stick} = 0.5$	(a)
	$\mu_{glide} = 0.2$	(a)
	$\mu_{limit} = 0.1$	(a)
	$v_{glide} = 1$ m s^{-1}	(a)
	$v_{limit} = 10$ m s^{-1}	(a)
	$s_{limit} = 100$ s m^{-1}	(a)

(a) Assumed; (b) Measured, Orona et al. (2017).

Table 2
Variables analyzed (Orona et al., 2017).

Variable	Mathematical representation	Eq.
Volume-averaged velocity of spheres	$\langle v_p \rangle = \frac{1}{V_T}\int_{V_T} \lvert \underline{v}_p \rvert \, dV_f$	(1)
Volume-averaged relative fluid velocity	$\langle v_{slip} \rangle = \frac{1}{V_T}\int_{V_T} v_{slip} \, dV_f = \frac{1}{V_T}\int_{V_T} \lvert \underline{v}_p - \underline{v}_f \rvert \, dV_f$	(2)
Volume-averaged turbulence intensity	$\langle Tu \rangle = \frac{1}{V_T}\int_{V_T} Tu \, dV_f$	(3)
Average minimum distance	$\langle d \rangle_t = \frac{\langle d_{\min} \rangle_t}{\langle d_{\min} \rangle_0} = \frac{1}{\langle d_{\min} \rangle_0} \sum_{i=1}^{E} \min_{i \neq j} \{d_{ij}\}_{j=1}^{E}$	(4)
Volume-averaged surface heat transfer coefficient	$\langle h_c \rangle = \frac{1}{V_T}\int_{V_T} h_c \, dV_f$	(5)
Time-averaged surface heat transfer coefficient	$\langle\langle h_c \rangle\rangle = \frac{1}{t_{Res}}\int_{t_{Res}} \langle h_c \rangle \, dt$	(6)

3.2. Velocity contours and streamlines

Fig. 2 shows illustrative velocity contours and streamlines of the cases studied. It is worth mentioning that results corresponding to $T = -5\,^{\circ}C$ are shown because a similar behavior was observed at $T = -10\,^{\circ}C$. An arbitrary cut plane is used to show the 3D information more easily. Moreover, the flow field corresponds to $t = 3\,s$, immediately before the injection of spheres.

In general, the velocity contours were similar to those described by Belis et al. (2015). High local velocities are observed close to the zones where jets are developed. Also, a higher number of orifices produce higher local velocities.

The analysis of the streamlines showed that the smallest number of orifices produced larger interaction zones among jets and recirculation zones. Also, jets were less perturbed as the number of orifices increased. It is

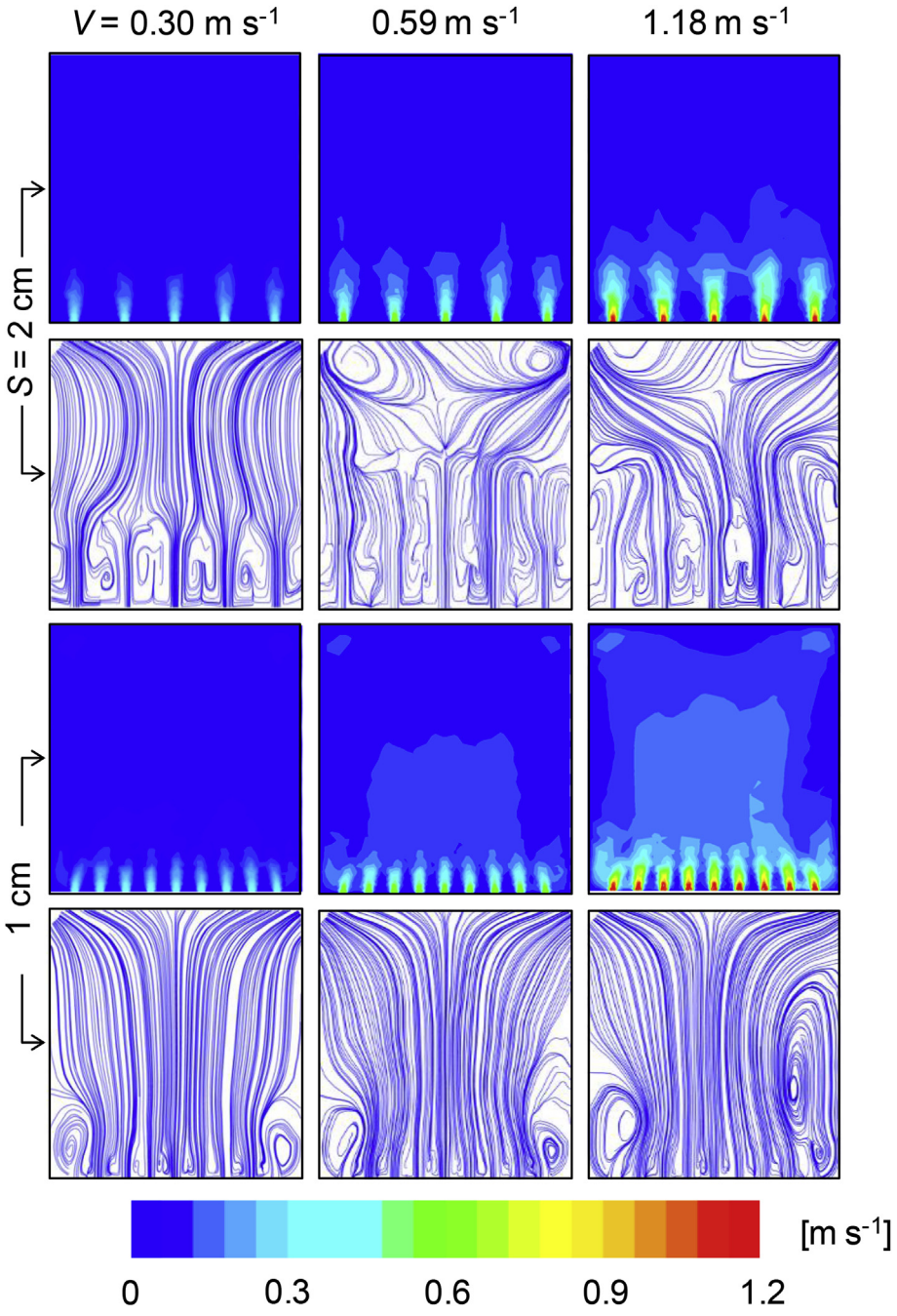

Fig. 2. Velocity contours and streamlines for the studied conditions and $t = 3\,s$ ($T = -5\,^{\circ}C$).

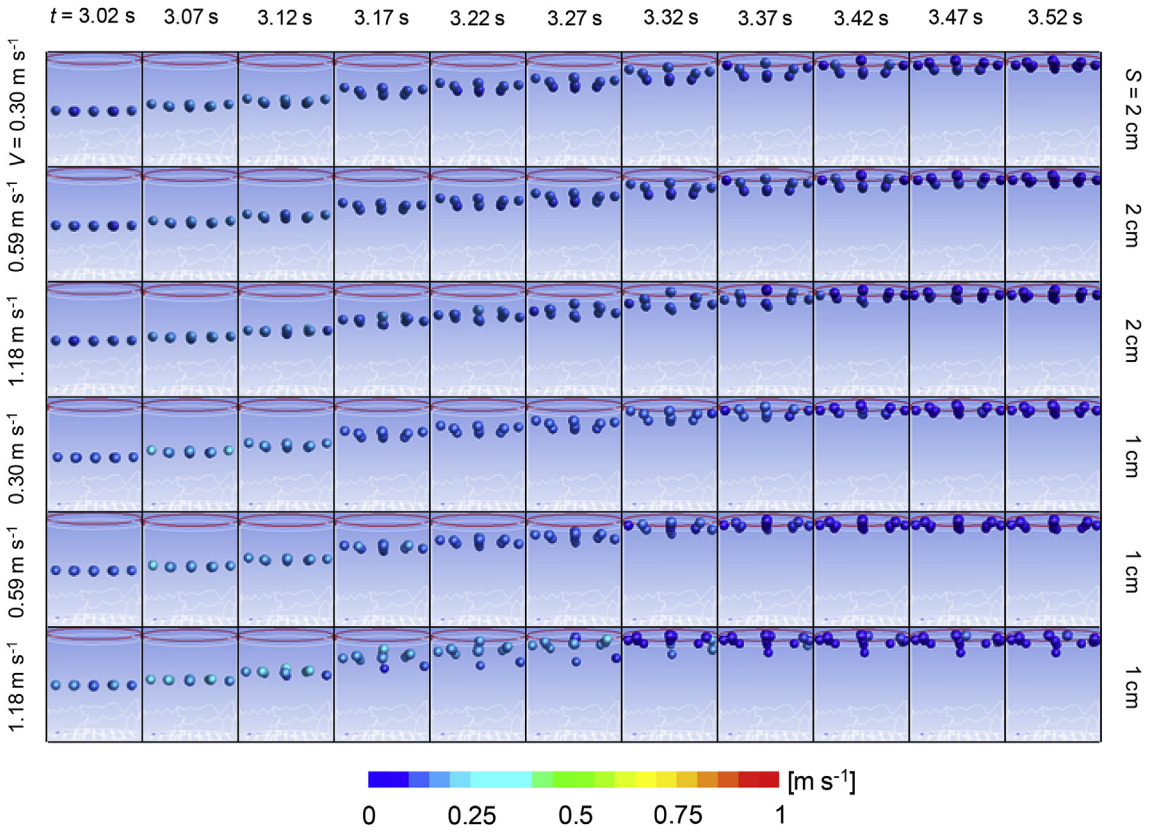

Fig. 3. Behavior of spheres after injection for the case $E = 13$ for the studied conditions ($T = -5\,^{\circ}C$). Color of spheres represents the velocity of spheres. (For interpretation of the references to colour in this figure legend, the reader is referred to the Web version of this article.)

important to mention that periodic eddies form and dissipate in the domain.

3.3. Behavior of spheres in the fluid domain

Figs. 3–5 show the behavior and the trajectories of the spheres after injection as a function of time. In general, it can be observed that spheres ascend at different velocities according to their initial position. In the cases of $E = 13$ and $E = 29$, the sphere trajectories are ascendant without descents. The relative velocities of the spheres are close related to the streamlines, that is, when a primary flow is observed ($S = 1$ cm), the fastest spheres are those injected in the central zone of the domain in agreement with the distribution of fluid velocities. The spheres injected close to the periphery are slower than those injected close to the domain axis. Moreover, a delay is observed due to the presence of eddies. When a secondary flow is observed ($S = 2$ cm), the spheres injected close to the domain periphery ascend faster following the canalization trend observed in the streamlines (Fig. 2). This behavior shows that for the cases $E = 13$ and $E = 29$, the spheres did not perturb the fluid field. All the spheres finished their ascending at the liquid-air interface approximately 1 s after being injected, and with similar initial distribution.

In the case of $E = 61$, the initial close distance of the spheres produces a rapid local increase of the fluid velocity when it passes between the free spaces of the initial array (Fig. 1*b*). This phenomenon produces the dispersion of spheres in axial and radial directions (Fig. 5). The spheres ascend faster close to the domain wall until reach the liquid-air interface ($t = 3.42$ s). In this case, due to the high number of spheres close to the domain exit, the fluid moves to the domain center. As a result, a secondary flow of liquid occurs while the spheres move downwards ($t = 3.62$ s). The secondary flow remains until find the main fluid flow close to the orifices, causing a direction change of the spheres and their ascent ($t > 3.82$ s). In general, an increase of V and a decrease of S produce an acceleration of the phenomena described. The effect of S was more pronounced than the effect of V.

3.4. Volume-averaged velocity of spheres

The volume-averaged velocity of spheres ($\langle v_p \rangle$) for the studied conditions as a function of time is shown in Fig. 6. For the cases $E = 13$ and $E = 29$, $\langle v_p \rangle$ increases to a maximum due to the initial contact of the spheres with the refrigerating medium. Then, an approximately plateau region is observed. Finally, a subsequent reduction to zero velocity values is obtained when the spheres reach the liquid-air interface.

The effect of the operative variables on the profiles of $\langle v_p \rangle$ was more pronounced for the case $E = 13$. The more important effect was the number of orifices, secondly the area-average fluid velocity at the orifices and marginally the temperature. In general, high values of $\langle v_p \rangle$ are obtained for small small S or high V and T. Small values of S produces

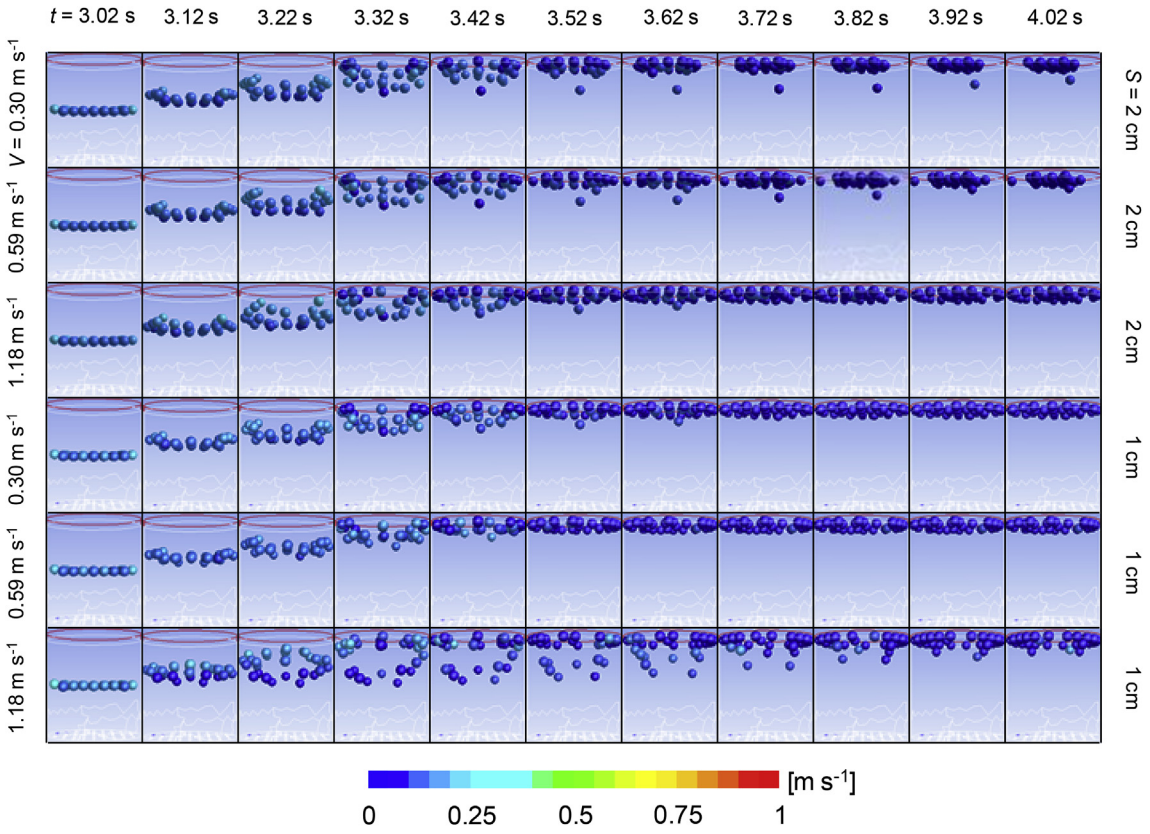

Fig. 4. Behavior of spheres after injection for the case $E = 29$ for the studied conditions ($T = -5\,^{\circ}C$). Color of spheres represents the velocity of spheres. (For interpretation of the references to colour in this figure legend, the reader is referred to the Web version of this article.)

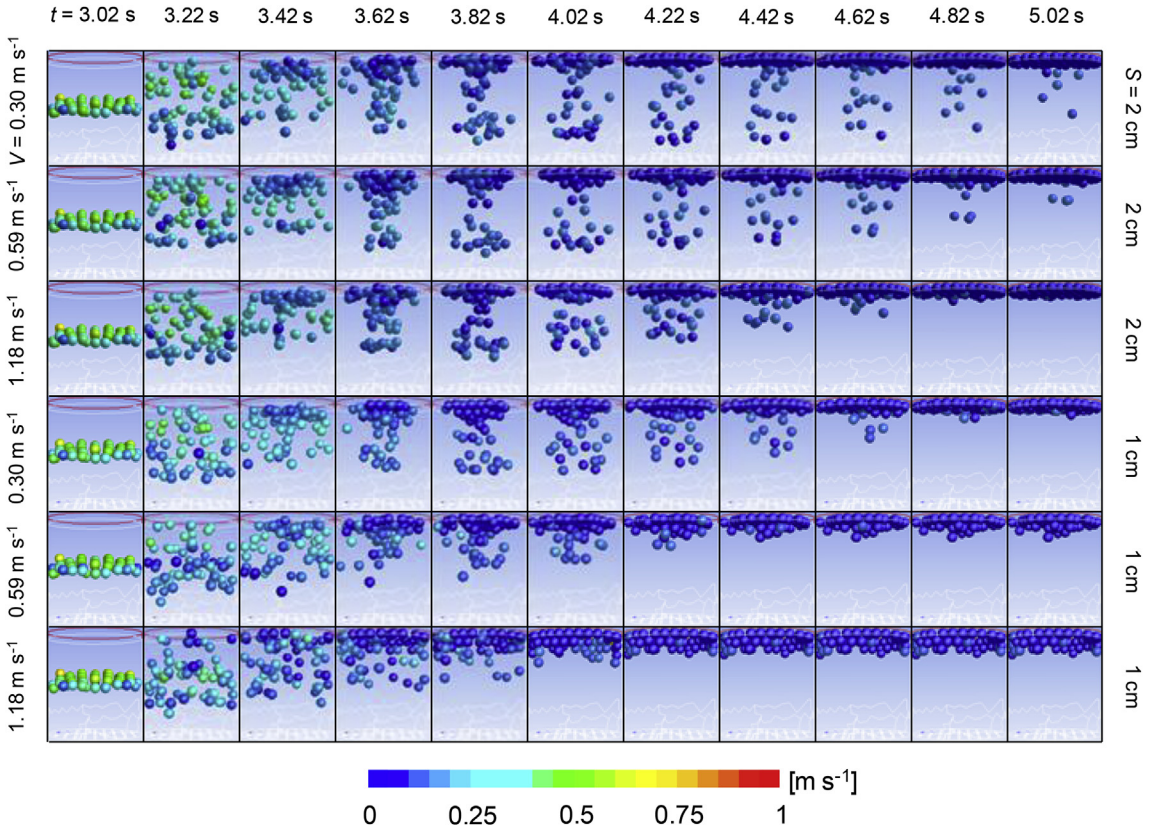

Fig. 5. Behavior of spheres after injection for the case $E = 61$ for the studied conditions ($T = -5\,^{\circ}C$). Color of spheres represents the velocity of spheres. (For interpretation of the references to colour in this figure legend, the reader is referred to the Web version of this article.)

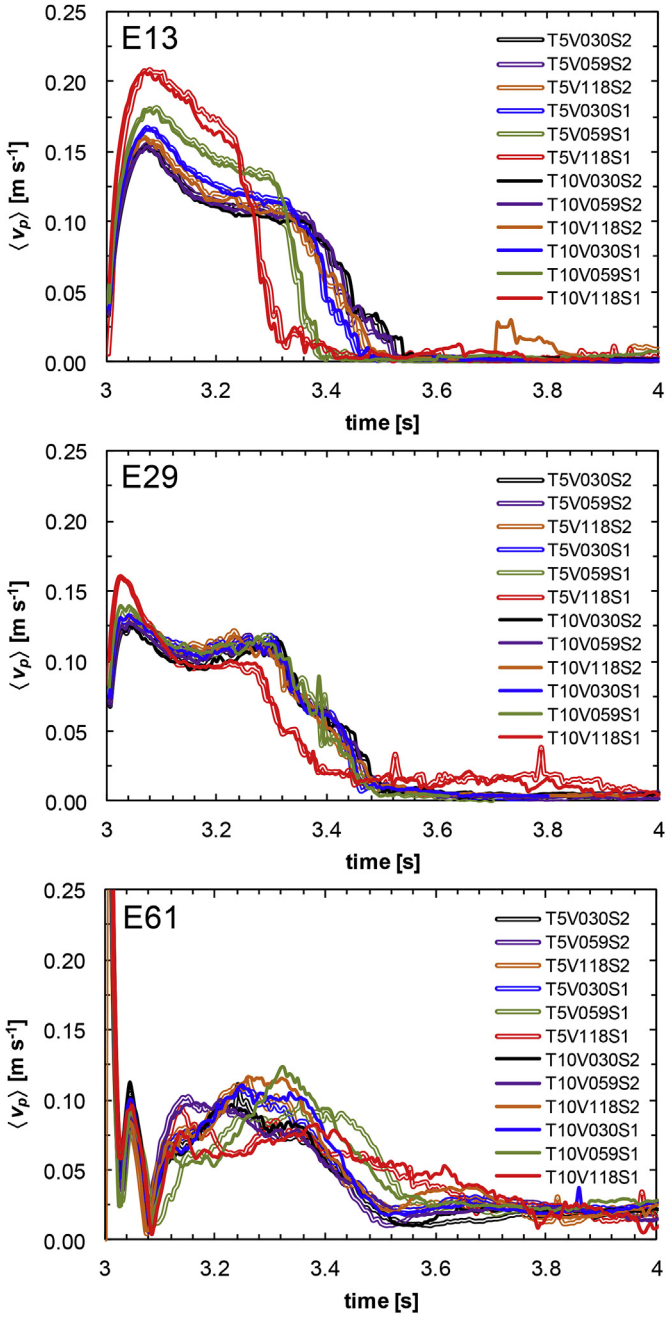

Fig. 6. Profiles of volume-averaged velocity of spheres ($\langle v_p \rangle$, Eq. (1)) for different number of spheres (E = 13, 29, 61) as function of time. The codification for T, V and S appears in the legend.

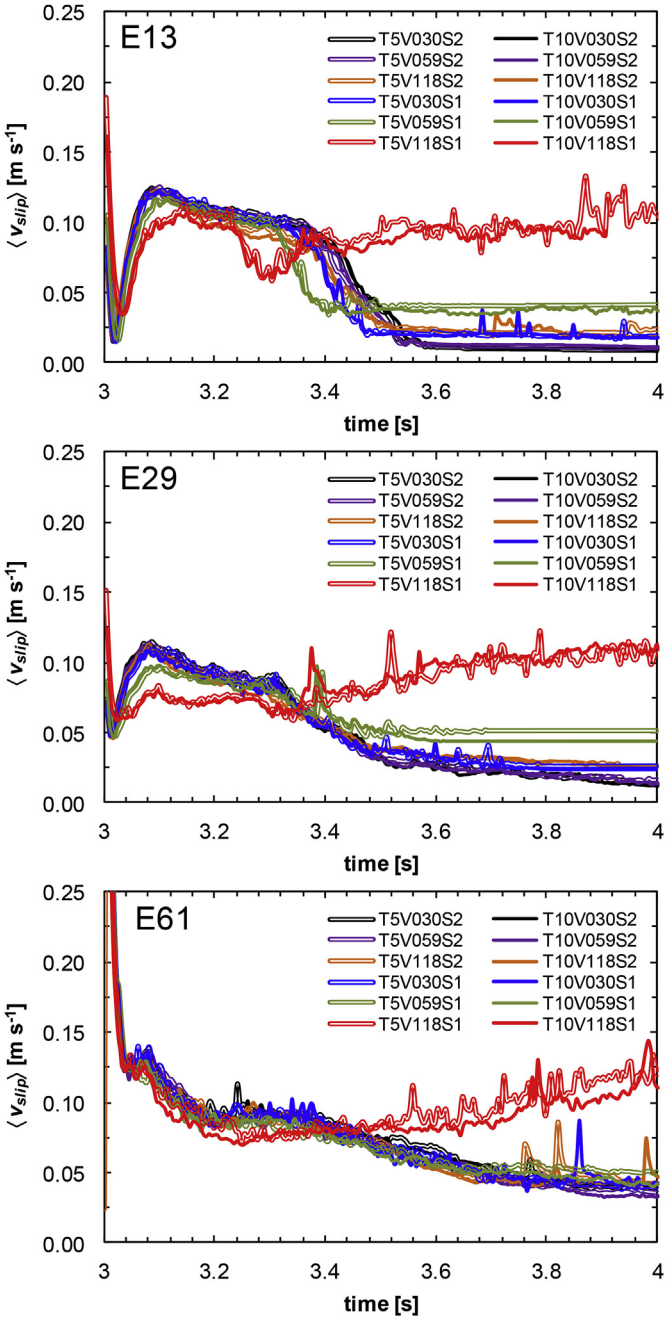

Fig. 7. Profiles of volume-averaged relative fluid velocity ($\langle v_{slip} \rangle$, Eq. (2)) for different number of spheres (E = 13, 29, 61) as function of time. The codification for T, V and S appears in the legend.

zones with high fluid velocities causing profiles with a higher maximum and a velocity decrease less pronounced. An increase in V produces a slight increment in the maximum and a shorter period of constant velocity due to the shorter residence time.

For the case E = 29, most of the profiles were similar except for the conditions S = 1 cm and V = 1.18 m s^{-1}. In that case, the synergic effect of the number of orifices and the fluid velocity produced a higher maximum in the profiles of $\langle v_p \rangle$.

It is interesting to notice that Fig. 6 also shows the representation of the displacement of spheres in the domain, that is, the integration of $\langle v_p \rangle$ over time. If the displacement of spheres is similar, the area under the curve of $\langle v_p \rangle$ will remain approximately similar. That effect is clearly observed for the cases E = 13 and E = 29, the sphere trajectory was almost vertical and the displacement was approximately equal to 0.05 m. For the case E = 61, the effect of the operative variables on the profiles of $\langle v_p \rangle$ is less noticeable.

3.5. Volume-averaged relative fluid velocity

The volume-averaged relative fluid velocity ($\langle v_{slip} \rangle$) for the studied

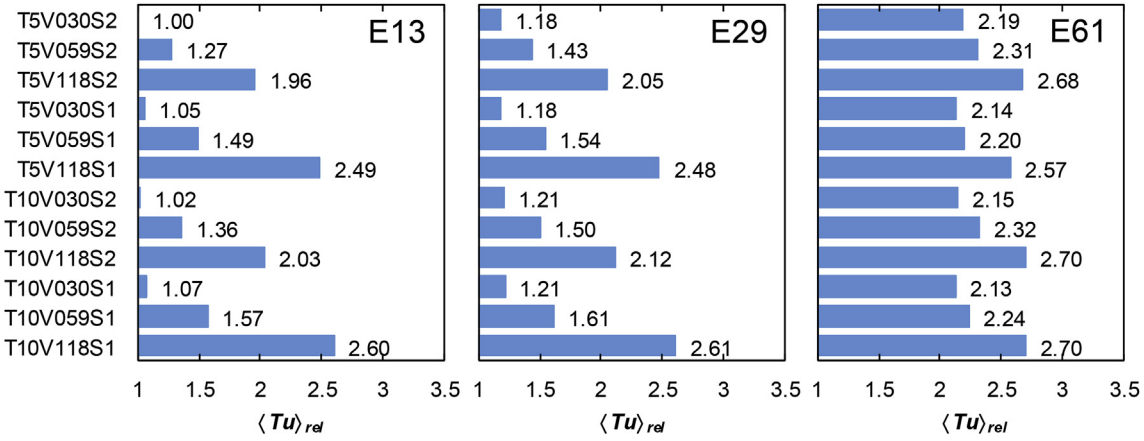

Fig. 8. Values of $\langle Tu \rangle_{rel}$ for different number of spheres ($E = 13, 29, 61$). The codification for T, V and S appears on the left of the graph. The reference condition is T5V030S2E13.

conditions as a function of time is shown in Fig. 7. For the cases $E = 13$ and $E = 29$, an initial velocity equal to the fluid velocity is observed at the injection point of the spheres due to the zero initial velocity of the spheres. A subsequent decrease is observed due to an initial velocity increment of the spheres and a slight decrease of the fluid velocity while the spheres ascend inside the domain. Then, a minimum is obtained when $\langle v_p \rangle$ and the fluid velocity are equaled. A zero value is obtained at this point but is not shown due to the time discretization used. Then, a second maximum is observed when spheres reached their maximum $\langle v_p \rangle$ (Fig. 6). Later, a slight decrease or plateau according to $\langle v_p \rangle$ profiles and small values of fluid velocity are obtained. Finally, a value of $\langle v_{slip} \rangle$ equal to the fluid velocity is obtained due to the spheres reached the liquid-air interface and $\langle v_p \rangle = 0$.

For the case $E = 61$, although both maxima of $\langle v_{slip} \rangle$ are observed, the decrease after the second maximum occurred because of the sphere dispersion (*i.e.* more spheres are placed in zones with low fluid velocities). Then, a plateau related to the upward movement of the spheres especially close to the wall domain is observed (Fig. 5). Finally, a continuous decrease during the secondary descendent flow and a later movement to the liquid-air interface are observed.

For all cases, when $V = 1.18\ \mathrm{m\,s^{-1}}$ and $S = 1$ cm, the initial characteristics of the $\langle v_{slip} \rangle$ profiles were similar to those of the other conditions studied. However, the final $\langle v_{slip} \rangle$ values were higher and no descendent behavior was observed.

The effect of the operative variables on the values of $\langle v_{slip} \rangle$ was similar to the one observed for the $\langle v_p \rangle$ profiles. In the case of $E = 13$, a decrease of S and an increase of V and T produce an increase in $\langle v_{slip} \rangle$. In the cases $E = 29$ and $E = 61$, the effects are less pronounced.

3.6. Turbulence levels

The effect of the operative variables on the turbulence levels was studied evaluating the relative turbulence at $t = 4$ s ($\langle Tu \rangle_{rel}$). This output was determined with the relation $\langle Tu \rangle / \langle Tu \rangle_{ref}$, where $\langle Tu \rangle_{ref}$ is the lowest turbulence level at $t = 4$ s. Fig. 8 shows the values of $\langle Tu \rangle_{rel}$ for the studied conditions. The condition T5V030S2E13 was selected as the reference condition.

The more important effect on $\langle Tu \rangle_{rel}$ corresponded to V , then S and then T. An increase in V and a decrease in S and T produce an increase in $\langle Tu \rangle_{rel}$. For the cases $E = 13$ and $E = 29$, the relations $\langle Tu \rangle_{rel} \cong 0.4(V/V_{\min})$, $\langle Tu \rangle_{rel} \cong -1.35(S/S_{\min})$ and $\langle Tu \rangle_{rel} \cong -0.39(T/T_{\min})$ are observed. The number of spheres in the cases $E = 13$ and $E = 29$ did not have a significant effect because the spheres did not considerably modify the fluid behavior (Figs. 3 and 4). In the case $E = 61$, the values of $\langle Tu \rangle_{rel}$ are higher due the number of spheres affected the fluid behavior, causing more eddies.

3.7. Dispersion level of the spheres

The dispersion level of the spheres measured through the average minimum distance ($\langle d \rangle_t$) as function of time for the conditions studied is shown in Fig. 9. The values of $\langle d \rangle_t$ increase until reaching a maximum for $3.2\ \mathrm{s} < t < 3.4\ \mathrm{s}$. The dispersion of spheres can be related to the interaction of spheres with the fluid, between them and with the walls. Then, a decrease of $\langle d \rangle_t$ is observed due to spheres are grouped together until reached the liquid-air interface.

For the case $E = 13$, the fluid carried the spheres without perturbing their initial position when $S = 2$ cm and for low values of V (Fig. 3). As a consequence, $\langle d \rangle_t$ remains almost constant with time. For the case $S = 1$ cm, as V increases, the values of $\langle d \rangle_t$ decrease faster. This behavior can be explained considering that a higher flow favors the grouping of spheres at liquid-air interface. However, spheres did not reach the value $\langle d \rangle_{t,\min} = 1/2$ during the period of time studied (*i.e.* spheres touched each other).

For the case $E = 29$, a decrease in $\langle d \rangle_t$ was observed after reaching the zone of maxima. For the case $S = 2$ cm, an increase in V produces less spheres grouping while ascending in the domain (Fig. 4). This behavior is not observed for $S = 1$ cm. In general, profiles converge to $\langle d \rangle_{t,\min} = 1/\sqrt{2}$ at different rates.

For the case $E = 61$, the profiles of $\langle d \rangle_t$ show a second region of maxima. This behavior is explained through the secondary flow of the fluid and spheres for $t > 3.62$ s (Fig. 5) that allows the spheres grouping in those streamlines and reaching lower values of $\langle d \rangle_t$. Then, $\langle d \rangle_t$ increases again due to the ascendant movement of the liquid. In general, profiles converge to $\langle d \rangle_{t,\min} = 1$ at different rates. It is important mentioning that the maxima observed for $t < 3.5$ s are higher for the case $S = 1$ cm. Moreover, the effect of V was more pronounced in these cases. This behavior can also be observed through the distribution of spheres in Fig. 5.

The higher the number of spheres, the higher the initial rate of increase in $\langle d \rangle_t$. This behavior can be explained considering that for a higher value of E, the spheres are closer each other and any movement produces a significant relative increment. In general, temperature did

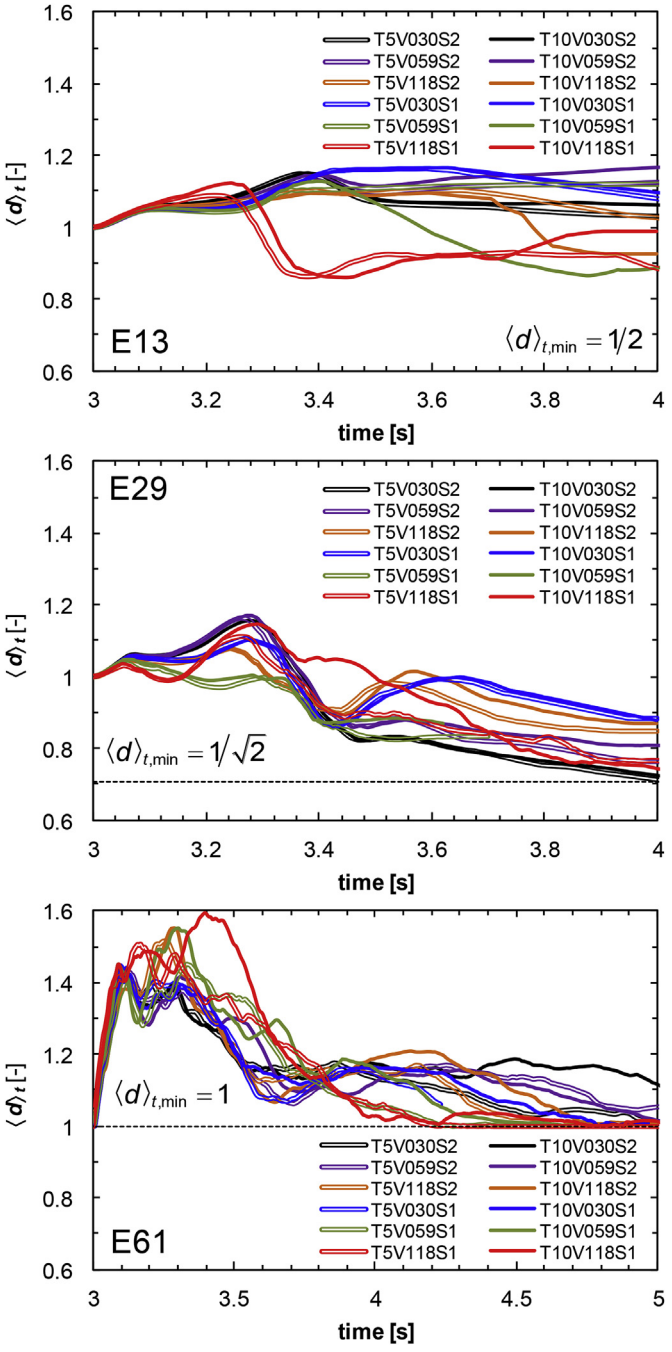

Fig. 9. Values of the dimensionless average minimum distance ($\langle d \rangle_t$, Eq. (4)) for different number of spheres (E = 13, 29, 61) as function of time. The codification for T, V and S appears in the legend.

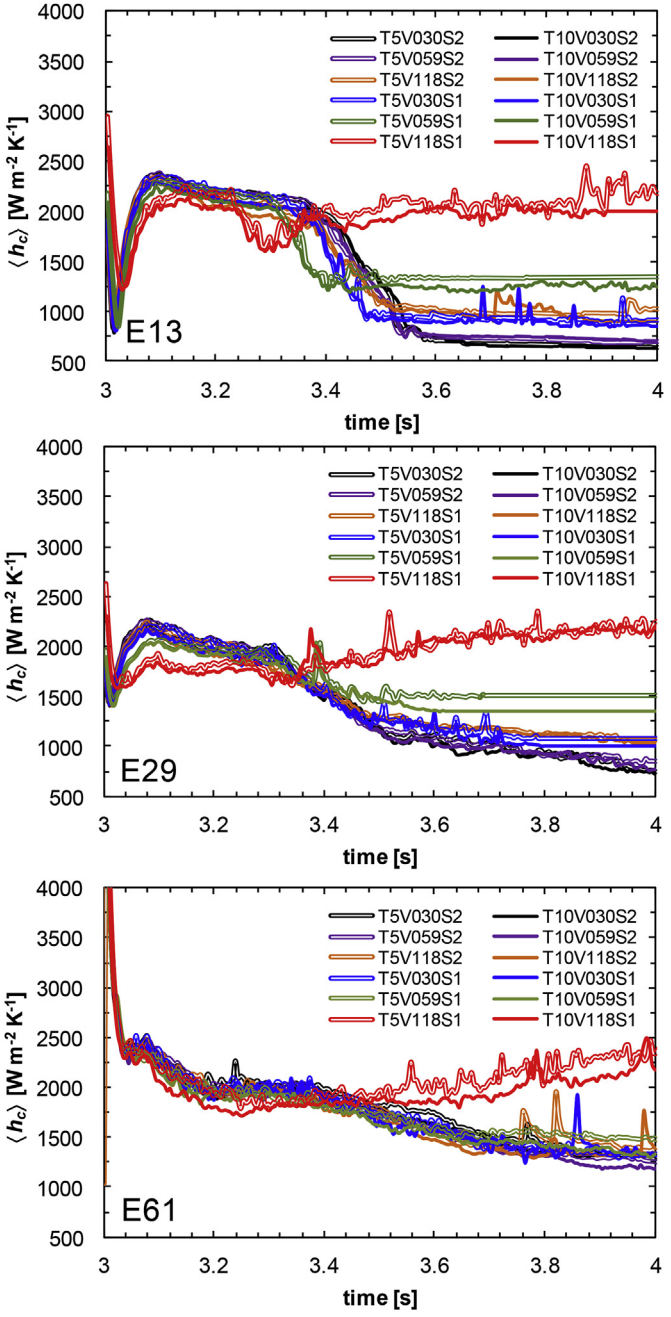

Fig. 10. Values of volume-averaged surface heat transfer coefficient ($\langle h_c \rangle$, Eq. (5)) for different number of spheres (E = 13, 29, 61) as function of time. The codification for T, V and S appears in the legend.

not show an important effect on the profiles of $\langle d \rangle_t$.

3.8. Surface heat transfer coefficient

The profiles of the volume-averaged surface heat transfer coefficient ($\langle h_c \rangle$) as a function of time for the studied conditions are shown in Fig. 10. Values are shown in the range of 3 s < t < 4 s. The behavior observed is similar to that observed for $\langle v_{slip} \rangle$ (Fig. 7) due to the relationship of these variables.

The time-averaged surface heat transfer coefficient $\langle\langle h_c \rangle\rangle$ was calculated for $t_{Res} = t_f - t_0 = 5$ s. In Table 3, the values of $\langle\langle h_c \rangle\rangle$ for the studied conditions are shown. An increment of E and V and a decrease

Table 3
Values of $\langle\langle h_c \rangle\rangle$ for the studied conditions.

Condition	$\langle\langle h_c \rangle\rangle$ [W m^{-2} K^{-1}]	Condition	$\langle\langle h_c \rangle\rangle$ [W m^{-2} K^{-1}]
T5V030S1E13	1009	T10V030S1E13	962
T5V030S1E29	1159	T10V030S1E29	1090
T5V030S1E61	1226	T10V030S1E61	1131
T5V030S2E13	780	T10V030S2E13	776
T5V030S2E29	875	T10V030S2E29	850
T5V030S2E61	1060	T10V030S2E61	1057
T5V059S1E13	1395	T10V059S1E13	1291
T5V059S1E29	1539	T10V059S1E29	1402
T5V059S1E61	1385	T10V059S1E61	1179
T5V059S2E13	831	T10V059S2E13	824
T5V059S2E29	964	T10V059S2E29	890
T5V059S2E61	1093	T10V059S2E61	1053
T5V118S1E13	2152	T10V118S1E13	1987
T5V118S1E29	2189	T10V118S1E29	2120
T5V118S1E61	2276	T10V118S1E61	2243
T5V118S2E13	1116	T10V118S2E13	1000
T5V118S2E29	1150	T10V118S2E29	1111
T5V118S2E61	1177	T10V118S2E61	1164

in S produce an increase in $\langle\langle h_c \rangle\rangle$. The effect of T on $\langle\langle h_c \rangle\rangle$ was marginal. In general, the relations $\langle\langle h_c \rangle\rangle/\langle\langle h_c \rangle\rangle_{\min} \cong 0.035(E/E_{\min})$, $\langle\langle h_c \rangle\rangle/\langle\langle h_c \rangle\rangle_{\min} \cong 0.2(V/V_{\min})$ and $\langle\langle h_c \rangle\rangle/\langle\langle h_c \rangle\rangle_{\min} \cong -1.7(S/S_{\min})$ were observed for the ranges of the conditions studied.

3.9. Mass and heat transfer in the food domain

The mass and heat transfer in the food domain was studied through the average NaCl concentration (C_{NaCl}) and through the temperature at the geometric center of the spheres (T_c), respectively (Peralta et al., 2012). Fig. 11*a* shows the profiles of C_{NaCl} as function of time for the different conditions studied. The refrigerating medium temperature was the variable with more important effect. The variables V, S and E did not have a noticeable effect. This behavior can be explained taking into account that the internal transport phenomena are mainly influenced by the temperature and that any variable combination ensures the decrease of the external mass transfer. It is worth mentioning that the C_{NaCl} values for the conditions at T = -5 °C were approximately 22% higher than for the conditions at T = -10 °C.

Fig. 11*b* shows the profiles of T_c for the studied conditions. The effect of the variables was similar to that observed for C_{NaCl}. To summarize the information, a characteristic freezing time necessary for the center to reach −4 °C (t_C) was defined (Belis et al., 2015). To compare the freezing times, a relative freezing time (t_R) was defined as the ratio of t_C at a certain condition to the t_C corresponding to the condition T10V118S1E61 (Fig. 12). The refrigerating medium temperature was the more important effect. An increase in temperature from −10 °C to −5 °C produces an increase of approximately 2.5 times in the values oft_R. An increase of 1 cm in S produces an increment of 6% in t_R, while a decrease to half V decreases 10% in t_R.

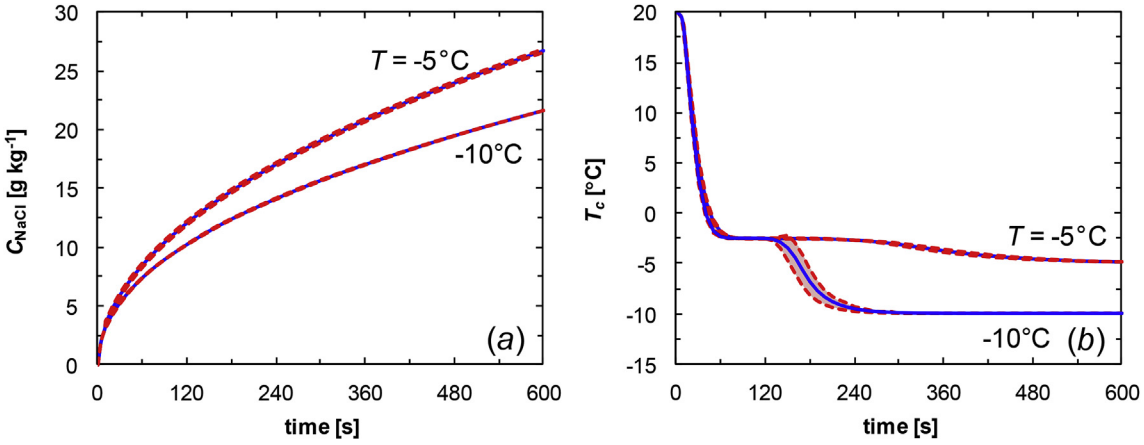

Fig. 11. (*a*) Average NaCl concentration and (*b*) temperature at the geometric center of spheres for the studied conditions grouped by the refrigerating medium temperature (T = −5 and −10 °C). Dashed lines represent the standard deviations.

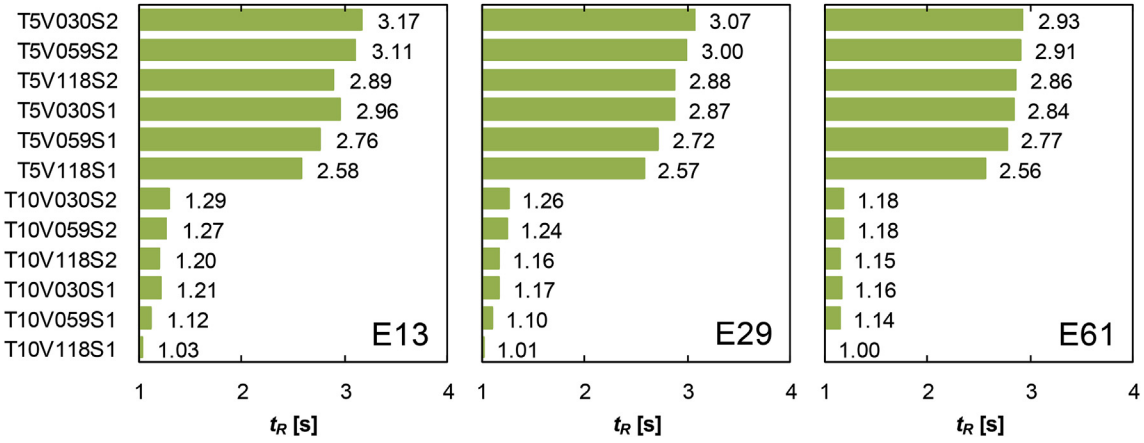

Fig. 12. Values of t_R for different number of spheres (E = 13, 29, 61). The codification for T, V and S appears on the left of the graph. The reference condition is T10V118S1E61.

4. Conclusions

Coupled CFD-DPM-DEM simulations were used to study a hydro-fluidization system with moving food spheres and multiple jets. The effect of operative variables (flow rate and temperature) and the number of spheres and orifices on representative variables of the momentum, heat and mass transfer was studied. In general, the number of spheres, the number of orifices and the averaged fluid velocity at the orifices were the main variables affecting the transfer phenomena in the fluid phase, while the refrigerating media temperature had a marginal effect. The energy transfer in the food domain was affected by all the variables analyzed, while the mass transfer was mainly affected by the refrigerating media temperature.

This study, involving a sensitivity analysis, shows that CFD-DPM-DEM is a powerful tool to perform relatively low cost simulations of food processing systems, allowing a more realistic description of the system. That is, essential variables (local and averaged) of heat and mass transfer can be estimated taking into account complex phenomena, such as fluidization and phase change processes. The general nature of the mathematical model presented here can be used by scientist, engineers and technicians to correctly design, develop, operate and optimize similar equipments and processes dealing with complex phenomena.

Acknowledgments

This research was supported partially by Universidad Nacional del Litoral (projects CAI + D: 501 201101 00031 LI and 504 201501 00002 LI) (Santa Fe, Argentina), Consejo Nacional de Investigaciones Científicas y Técnicas (project PIP 2015–2017 11220150100185) (Argentina), and Agencia Nacional de Promoción Científica y Tecnologica (projects ANPCyT: 2011-182, 2012-1413, 2015-365) (Argentina).

Nomenclature

A_y	cross sectional area to the domain axis at the height y [m^2]
C_{NaCl}	volume-averaged NaCl concentration in the potato spheres [g Kg^{-1}]
D	diameter of the spheres [cm]
d	diameter of the orifices [cm]
d_{ij}	Euclidean distance of geometric centers [m]
$\langle d \rangle_t$	dimensionless average minimum distance defined by Eq. (4) [−]
$\langle d \rangle_{t,\min}$	minimum value of $\langle d \rangle_t$ for a certain condition [−]
$\langle d_{\min} \rangle_t$	average minimum distance at t defined in Eq. (4) [m]
$\langle d_{\min} \rangle_0$	value of $\langle d_{\min} \rangle_t$ at t = 0 s defined in Eq. (4) [m]
E	number of spheres [−]
$E_{\min}$	minimum value of E [−]
F_D	drag force per unit sphere mass [m s^{-2}]
$\underline{F}_{DEM}$	force per unit sphere mass due to the interactions between spheres estimated by DEM [m s^{-2}]
$\underline{F}_N$	normal component of $\underline{F}_{DEM}$ [m s^{-2}]
$\underline{F}_T$	tangential component of $\underline{F}_{DEM}$ [m s^{-2}]
H_0	initial position of spheres relative to the orifice plate [mm]
h_c	surface heat transfer coefficient [W m^{-2} K^{-1}]
$\langle h_c \rangle$	volume-averaged surface heat transfer coefficient define by Eq. (5) [W m^{-2} K^{-1}]
$\langle\langle h_c \rangle\rangle$	time-averaged $\langle h_c \rangle$ defined by Eq. (6) [W m^{-2} K^{-1}]
$\langle\langle h_c \rangle\rangle_{\min}$	minimum value of $\langle\langle h_c \rangle\rangle$ [W m^{-2} K^{-1}]
K	spring constant per unit mass [s^{-2}]
S	minimum distance between the geometric centers of the orifices [cm]
$S_{\min}$	minimum value of S [cm]
s_{limit}	parameter determining how fast $\mu_{friction}$ approaches μ_{limit} [s m^{-1}]
T	refrigerating medium temperature [°C]
T_c	temperature of the geometric center of the spheres [°C]
$T_{\min}$	minimum value of T [°C]
t	time [s]
t_0	initial time [s]
t_C	characteristic freezing time necessary for T_c = -4 °C [s]
t_f	final time [s]
t_R	ratio of t_C to t_C for T10V118S1E61 [-]
t_{Res}	total residence time of the spheres in the domain [s]
Tu	local turbulence intensity ($\sqrt{\frac{2}{3}\kappa}/\lvert\underline{v}_f\rvert$) [−]
$\langle Tu \rangle$	volume-averaged Tu defined by Eq. (3) [−]
$\langle Tu \rangle_{rel}$	ratio of $\langle Tu \rangle$ to $\langle Tu \rangle_{ref}$ [−]
$\langle Tu \rangle_{ref}$	minimum value of $\langle Tu \rangle$ evaluated at t = 4 s [−]
V	area averaged fluid velocity at the orifices [m s^{-1}]
V_f	refrigerating medium volume [m^3]
$V_{\min}$	minimum value of V [m s^{-1}]
V_T	volume of the fluid domain [m^3]
$\underline{v}_f$	fluid velocity vector [m s^{-1}]
$\underline{v}_p$	sphere velocity vector [m s^{-1}]
v_{glide}	gliding velocity [m s^{-1}]
v_{slip}	magnitude of $\underline{v}_p - \underline{v}_f$ [m s^{-1}]
v_{limit}	limit velocity [m s^{-1}]
$\langle v_f \rangle$	area-averaged $\lvert\underline{v}_f\rvert$ at A_y[m s^{-1}]
$\langle v_p \rangle$	volume-averaged $\lvert\underline{v}_p\rvert$ defined by Eq. (1) [m s^{-1}]
$\langle v_{slip} \rangle$	volume-averaged v_{slip} defined by Eq. (2) [m s^{-1}]
x, y, z	Cartesian coordinates [m]

Greek symbols

η_p	coefficient of restitution for sphere-sphere interactions [−]
η_w	coefficient of restitution for sphere-wall interactions [−]
κ	turbulence kinetic energy [$m^2\ s^{-2}$]
$\mu_{friction}$	friction coefficient [−]
μ_{glide}	gliding friction coefficient [−]
μ_{limit}	high velocity limit friction coefficient [−]
μ_{stick}	sticking friction coefficient [−]
ω	specific turbulence dissipation rate [s^{-1}]

Acronyms

CFD	computational fluid dynamics
DEM	discrete element method
DPM	discrete phase method
HF	hydrofluidization

References

Belis, E.E., Zorrilla, S.E., Peralta, J.M., 2015. Effect of the number of orifices and operative variables on the heat and mass transfer in a hydrofluidization system with static spheres. J. Food Eng. 153, 96–107. https://doi.org/10.1016/j.jfoodeng.2014.12.016.

Crowe, C.T., Schwarzkopf, J.D., Sommerfeld, M., Tsuji, Y., 2012. Multiphase Flows with Droplets and Particles, second ed. CRC Press, Boca Raton, FL.

Fikiin, A.G., 1992. New method and fluidized water system for intensive chilling and freezing of fish. Food Contr. 3, 153–160. https://doi.org/10.1016/0956-7135(92)90100-O.

Fikiin, K., 2008. Emerging and novel freezing processes. In: Evans, J.A. (Ed.), Frozen Food Science and Technology. Blackwell Publishing Ltd., Oxford, UK, pp. 101–123.

Fikiin, K., 2003. Novelties of Food Freezing Research in Europe and beyond. Flair-flow Europe Synthetic Brochure for SMEs no.10. Institut National de la Recherche Agronomique, Paris, France.

Fikiin, K., Fikiin, A., 1998. Individual quick freezing of foods by hydrofluidisation and pumpable ice slurries. In: Fikiin, K. (Ed.), IIR Proceedings Series "Refrigeration Science and Technology." Presented at the International Conference on Advances in the Refrigeration Systems, Food Technologies and Cold, pp. 319–326. Sofia, Bulgaria. https://doi.org/10.13140/RG.2.1.3901.1283/1.

Fryer, P.J., Porras-Parral, G., Bakalis, S., 2011. Multiphysics modeling of ohmic heating. In: Knoerzer, K., Juliano, P., Roupas, P., Versteeg, C. (Eds.), Innovative Food Processing Technologies: Advances in Multiphysics Simulation. Blackwell Publishing Ltd., Oxford, UK, pp. 155–169.

Gidaspow, D., 1994. Multiphase Flow and Fluidization: Continuum and Kinetic Theory Descriptions. Academic Press, Boston, MA.

James, C., Purnell, G., James, S.J., 2015. A review of novel and innovative food freezing technologies. Food Bioprocess Technol. 8, 1616–1634. https://doi.org/10.1007/s11947-015-1542-8.

Norton, T., Sun, D.-W., 2010. CFD: an innovative and effective design tool for the food industry. In: Aguilera, J.M., Simpson, R., Welti-Chanes, J., Bermudez-Aguirre, D., Barbosa-Canovas, G. (Eds.), Food Engineering Interfaces. Springer New York, New York, NY, pp. 45–68. https://doi.org/10.1007/978-1-4419-7475-4_3.

Norton, T., Sun, D.-W., 2007. An Overview of CFD Applications in the Food Industry. In: Sun, D.-W. (Ed.), Computational Fluid Dynamics in Food Processing. CRC Press, Boca Raton, FL, pp. 1–41.

Orona, J.D., Zorrilla, S.E., Peralta, J.M., 2017. Computational fluid dynamics combined with discrete element method and discrete phase model for studying a food hydrofluidization system. Food Bioprod. Process. 102, 278–288. https://doi.org/10.1016/j.fbp.2017.01.005.

Peralta, J.M., Rubiolo, A.C., Zorrilla, S.E., 2012. Mathematical modeling of the heat and mass transfer in a stationary potato sphere impinged by a single round liquid jet in a hydrofluidization system. J. Food Eng. 109, 501–512. https://doi.org/10.1016/j.jfoodeng.2011.10.032.

Peralta, J.M., Rubiolo, A.C., Zorrilla, S.E., 2010. Mathematical modeling of the heat transfer and flow field of liquid refrigerants in a hydrofluidization system with a stationary sphere. J. Food Eng. 99, 303–313. https://doi.org/10.1016/j.jfoodeng.2010.03.003.

Peralta, J.M., Rubiolo, A.C., Zorrilla, S.E., 2009. Design and construction of a hydrofluidization system. Study of the heat transfer on a stationary sphere. J. Food Eng. 90, 358–364. https://doi.org/10.1016/j.jfoodeng.2008.07.004.

Peralta, J.M., Rubiolo, A.C., Zorrilla, S.E., 2007. Prediction of heat capacity, density and freezing point of liquid refrigerant solutions using an excess Gibbs energy model. J. Food Eng. 82, 548–558. https://doi.org/10.1016/j.jfoodeng.2007.03.010.

Thévenin, D., Janiga, G. (Eds.), 2008. Optimization and Computational Fluid Dynamics. Springer Berlin Heidelberg, Berlin, Heidelberg. https://doi.org/10.1007/978-3-540-72153-6.

Tsotsas, E., Mujumdar, A.S., 2014. Modern Drying Technology. Process intensification. vol. 5 Wiley-VCH, Weinheim, Germany.

Verboven, P., Scheerlinck, N., Nicolaï, B.M., 2003. Surface heat transfer coefficients to stationary spherical particles in an experimental unit for hydrofluidisation freezing of individual foods. Int. J. Refrig. 26, 328–336. https://doi.org/10.1016/S0140-7007(02)00110-X.

Zorrilla, S.E., Rubiolo, A.C., 2005a. Mathematical modeling for immersion chilling and freezing of foods: Part I: model development. J. Food Eng. 66, 329–338. https://doi.org/10.1016/j.jfoodeng.2004.03.026.

Zorrilla, S.E., Rubiolo, A.C., 2005b. Mathematical modeling for immersion chilling and freezing of foods: Part II: model solution. J. Food Eng. 66, 339–351. https://doi.org/10.1016/j.jfoodeng.2004.03.027.